Combustion efficiency of a porous injector during throttling of a LOX/H_2 combustion chamber

J. Deeken, D. Suslov, O. Haidn, S. Schlechtriem
German Aerospace Center (DLR)
Institute of Space Propulsion
Langer Grund, 74239 Hardthausen, Germany

Abstract

The effect of throttling on combustion efficiency and stability of a porous injector head has been investigated for the propellant combination LOX/H_2. Several pressure ramps ranging from 30 bar to 100 bar have been used so that a broad range of possible chamber pressures was covered. Regarding the design pressure of 80 bar this was equivalent to a throttling range of 37.5 % to 125 %. The hydrogen injection temperature was varied between 50 K and 105 K. The oxygen injection temperature was about 115 K ± 5 K. All tests were performed at the test bench P8 using a 50 mm diameter modular combustion chamber. The combustion efficiency at a hydrogen injection temperature of 105 K varied between 97.5 % and 99 % and is nearly independent of the pressure. For hydrogen at 50 K the combustion efficiency increases with increasing chamber pressure and ranges from 94 % to 97 %. The combustion roughness at 50 K is higher than for the 105 K test cases.

1. Introduction

1.1 Requirements

The key requirement for a useful injector head is its operational flexibility, i.e. the ability to operate over a broad range of thrust levels without a major degradation of combustion efficiency and combustion stability. Certain proposed missions, e.g. lander missions, require an engine which delivers a specific thrust at a certain time of the flight profile. The engine for the Apollo lunar lander can be throttled to 10 % of its nominal thrust.[1] At the same time a degradation of the performance due to throttling has to be avoided. Conventional coaxial injector elements rely on the momentum exchange between the fuel and the oxidizer due to shear forces for the primary atomization. Injector element dimensions are optimized for a certain small operating range. Typical injection velocities are $v_{H_2} = 200 - 300\,\mathrm{m/s}$ and $v_{O_2} = 20 - 30\,\mathrm{m/s}$. For a constant injector geometry, the relevant hydrodynamic parameters of injection, like the velocity ratio of fuel and oxidizer $VR = v_f/v_o$ or the momentum flux ratio $J = (\rho_f v_f^2)/(\rho_o v_o^2)$, vary with changing combustion chamber pressure. The chamber pressure is roughly proportional to the delievered thrust. A deep throttling of an engine which is equipped with coaxial injector elements would cause an operation at non-nominal conditions which leads to a degradation of performance.[4] An injector design which is insensitive to the varying injection conditions is preferable for applications which require throttling capability.

1.2 API approach

At the DLR Institute of Space Propulsion Lampoldshausen an injector head design is investigated which relies on an increased initial contact surface between the fuel and the oxidizer to promote atomization, while classical injector heads with coaxial elements rely on shear forces close to the injector head. The increase in the contact surface between the fuel and the oxidizer is achieved by injecting the oxidizer (LOX, Liquid OXygen) through many small tubes in a parallel showerhead configuration. The individual LOX jet diameter for the injector head which is presented here is 1.5 mm. The fuel - in this case hydrogen - is injected through a porous faceplate. Further on, this assembly will be called API. Due to the large injection area, hydrogen injection velocities are very low. Typically they are in the range of 4 m/s to 12 m/s, depending on the injection temperature. LOX injection velocities typically range between 5 m/s and 17 m/s for chamber pressures of 30 bar and 100 bar, respectively. Since no significant propellant acceleration by

the injector head is needed for the atomization, the pressure drops for the fuel and the oxidizer across the injector can be kept comparably low. For hydrogen temperatures of 105 K, the hydrogen pressure drop across the faceplate was below 10 % of the chamber pressure. For lower hydrogen injection temperatures, the hydrogen pressure drop decreases further. The opportunity to design for low hydrogen pressure drops has several advantages regarding the design of an engine. With the API concept the engine cycle can be optimised by either an increased chamber pressure or a more efficient turbopump.
Due to the small difference in velocity between the LOX jet and the surrounding H_2, initial Weber numbers are very low compared to coaxial injectors. For a porous injector using the API design the atomization is dominated by the disintegration of the LOX jet by the accelerating combustion gases. The velocity difference between the oxygen jets and the combustion gases increases rapidly with axial distance from the injector head and is promoting mixing by shear forces. The axial mean velocity profile for the combustion gases is an important parameter for the atomization. Figure 1 shows results of the static pressure measurements along the wall. At a location 130 mm downstream of the injector faceplate the chamber pressure converges to a near constant value. Propellant reaction and acceleration of the combustion gases is essentially complete at this axial position and the chamber velocity approaches the value which is theoretically determined by a CEA calculation. The combustion gases are accelerated from nearly zero velocity to about 320 m/s within a distance of 130 mm. In principle, the task of mixing of the propellants is transfered from the injector head to the combustion process itself.

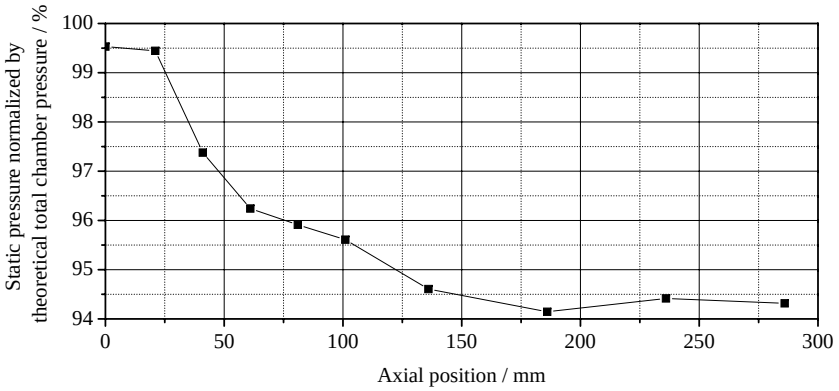

Figure 1: Axial pressure distribution for PR III (see 2.2) at 80 bar theoretical total chamber pressure

2. Experimental Setup

2.1 Combustion Chamber and Sensor Equipment

The data presented in this paper was determined using the DLR subscale combustion chamber model B and the porous injector head API68.[2] The LOX is injected via 68 small diameter tubes ($d_{\text{outer}}/d_{\text{inner}} = 2.0\,\text{mm}/1.5\,\text{mm}$) while the fuel is injected through the whole area of the porous faceplate. The modular combustion chamber with a diameter of $d_{\text{cc}} = 50\,\text{mm}$ consists of one measurement segment (length: 100 mm), four standard segments (length: 50 mm) and a nozzle segment with a throat diameter of 28 mm. The contraction ratio is $\epsilon_{\text{c}} = A_{\text{cc}}/A_{\text{t}} \approx 3.19$. The total combustion chamber length is 328 mm with a value of $L^* = 1009\,\text{mm}$. The 100 mm measurement segment features 9 static pressure sensors with an axial spacing of 10 mm, which allows for a high spatial resolution regarding the static pressure measurements. In addition to these static pressure sensors one dynamic pressure sensor and one thermocouple close to the chamber wall are employed in the measurement segment. All standard 50 mm segments are equipped with one static pressure sensor, one dynamic pressure sensor and one thermocouple, each positioned at half the length of the segment. Each segment is water cooled. A calorimetric determination of the heat flux in a segment is possible due to the application of thermocouples and flow meters in the individual water feed lines. Static as well as dynamic pressure sensors are located about 200 mm away from the combustion chamber and are connected via tubes with an inner diameter of 4 mm. This volume inside the connecting tubes acts as a damper for pressure oscillations. Thus, the amplitude measurements are unreliable and can only be used as a qualitative information. Measured frequencies are not affected by this effect. The data from the static pressure sensors was sampled at a rate of 100 Hz, while the dynamic pressure data was sampled at 100 kHz.

Alternating the position of the measurement segment allows for high resolution pressure measurements at any axial position in the combustion chamber. The arrangement in which the measurement segment is located directly behind the injector head (position: 0-100 mm) will be designated configuration I, while the configuration in which the measurement segment is located at an axial position of 100-200 mm will be referred to as configuration II.
Due to the encouraging results of an application of an uncooled sensor ring which was located directly downstream of the injector head during a test campaign with the combustion chamber model G, later test runs also used such a sensor ring. This uncooled copper ring (length: 11 mm) is equipped with four dynamic pressure sensors at certain angular positions to allow for a phase determination in case transversal modes of a combustion instability are detected. The use of this additional sensor ring increases the combustion chamber length to 339 mm and the value of L^* to 1044 mm. The position of the chamber segments is identical to configuration I. This arrangement will be referred to as configuration III. The dynamic pressure sensors applied in the sensor ring are located 10 mm away from the combustion chamber. Former experiments with combustion chamber G indicated that a closer distance is likely to endanger the sensor. The enclosed volume of combustion gases in the 10 mm long cavity is considered small enough to have a negligible effect on pressure amplitude measurements. The described configurations are displayed in table 1. The test runs presented in this paper were performed with configurations II and III.

Table 1: Combustion Chamber Configurations

Configuration	Segments used	Throat diameter	Contraction ratio	Chamber lenght to throat	$L*$
I	measurement segment, 4 standard segments, nozzle	28 mm	3.19	328 mm	1009 mm
II	2 standard segments, measurement segment, 2 standard segments, nozzle	28 mm	3.19	328 mm	1009 mm
III	HF sensor ring, measurement segment, 4 standard segments, nozzle	28 mm	3.19	339 mm	1044 mm

2.2 Operating Conditions

In order to investigate the throttling capability of the described injector head, multiple test runs have been performed. Pressure ramps (PR), which vary the chamber pressure at a constant rate by a variation of the propellant mass flow allow for investigation of combustion efficiency and stability over a wide range of operating conditions. The nominal point of operation for the investigated API injector head was 80 bar. A pressure ramp ranging from 30 bar to 100 bar leads to a throttling range of 37.5 % to 125 %. Injection conditions for three pressure ramps are presented in table 2. All values except pressure are the minimum and maximum values encountered during the ramp test. PR I was performed using hydrogen at approximately 50 K ('liquid' hydrogen, LH_2) and the pressure was varied at a rate of 2 bar/s. PR II and PR III used the same sequence and target values for pressures, temperatures and mass flow rates. Hydrogen was injected at approximately 105 K and the pressure change rate was -1 bar/s. PR II used the chamber configuration II (without the sensor ring), while PR III used the chamber configuration III (with the sensor ring). Static pressure readings at the faceplate are presented in figure 2. Before and after each pressure ramp, injection conditions were held constant for at least five seconds, which ensures thermal equilibrium in the chamber.

Table 2: Operating Conditions

	Configuration	p_{cc} / bar	ROF	T_{H_2} / K	T_{O_2} / K
PR I	III	30 ... 100	4.96 ... 5.01	47.4 ... 53.3	113.4 ... 119.3
PR II	II	100 ... 30	4.85 ... 5.31	99 ... 110.7	113.3 ... 117.6
PR III	III	100 ... 30	4.75 ... 5.17	99.4 ... 110.5	112.8 ... 117.5

	u_{Inj,H_2} / m/s	u_{Inj,O_2} / m/s	Re_{Inj,O_2}	1-L mode / Hz	1-T mode / Hz
PR I	3.9 ... 9.6	5.4 ... 16.9	75469 ... 212130	2405 ... 2438	16306 ... 16527
PR II	9.6 ... 11.9	5.3 ... 17.2	69765 ... 224681	2484 ... 2534	16294 ... 16623
PR III	9.8 ... 11.9	5.3 ... 17.2	69759 ... 224200	2395 ... 2454	16236 ... 16636

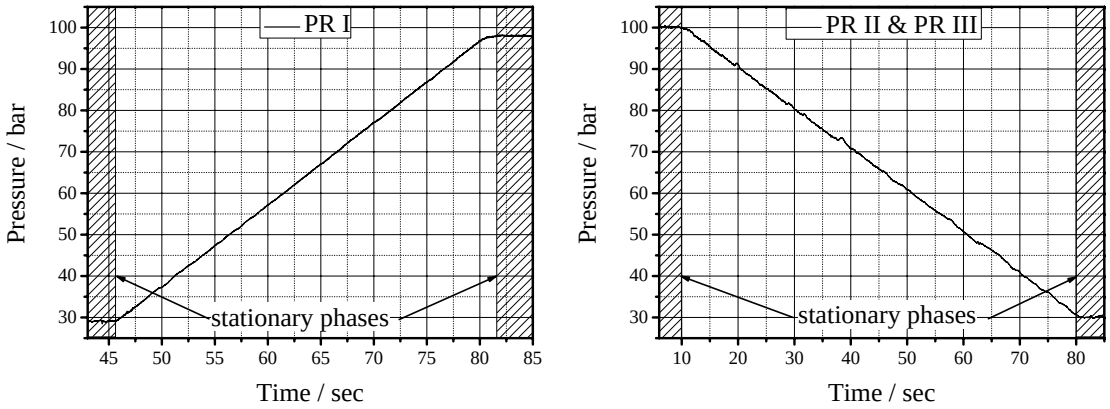

Figure 2: Static pressure at the faceplate

3. Experimental Results

3.1 Combustion Efficiency

3.1.1 Analysis

In order to measure the quality of the whole combustion process in a rocket combustion chamber, the characteristic velocity c^* is introduced and defined as

$$c^* = \frac{p_{0,\mathrm{cc}} A_\mathrm{t}}{\dot{m}} \tag{1}$$

With the characteristic velocity an efficiency η_{c^*} is defined.

$$\eta_{c^*} = \frac{c^*_\mathrm{exp}}{c^*_\mathrm{theo}} \tag{2}$$

This efficiency represents the ratio of the experimentally achieved value for c^* and the theoretically possible value. The theoretical value for c^*_theo or $p_{0,\mathrm{theo}}$ is obtained by assuming a complete combustion of all propellants and chemical equilibrium in the combustion chamber. The ideal combustion chamber values are computed using NASA's CEA code. This code assumes zero injection velocity for the calculation of $p_{0,\mathrm{theo}}$. Since the mass flow rate and the nozzle throat area are equal for the theoretical and the experimental case, the calculation of η_{c^*} reduces to

$$\eta_{c^*} = \frac{p_{0,\mathrm{exp}}}{p_{0,\mathrm{theo}}} = \frac{p_{0,\mathrm{EOC,exp}}}{p_{0,\mathrm{EOC,theo}}} \tag{3}$$

For efficiency determination a pressure sensor is chosen which is located directly ahead of the nozzle contraction. This location is named EOC (End Of Combustion). The measured static pressure has to be related to a total pressure at this axial position, while the theoretical total pressure determined for a negligible chamber velocity has to be corrected for total pressure losses due to the nonisentropic nature of the combustion. This correction is justified since the losses in total pressure due to nonisentropic combustion can not be attributed to the injector head but to the combustion chamber contraction ratio.[3] The Mach number at the location EOC is determined by using the contraction ratio and the ratio of the specific heats γ_EOC. The acceleration in the nozzle contraction is assumed to be isentropic.

$$\epsilon_\mathrm{c} = \frac{A_\mathrm{cc}}{A_\mathrm{t}} = \frac{1}{M_\mathrm{EOC}} \left[\frac{2}{\gamma_\mathrm{EOC}+1} \left(1 + \frac{\gamma_\mathrm{EOC}-1}{2} M^2_\mathrm{EOC} \right) \right]^{\frac{\gamma_\mathrm{EOC}+1}{2(\gamma_\mathrm{EOC}-1)}} \tag{4}$$

The ratio of the total and the static pressure at the location EOC is

$$\frac{p_{0,\mathrm{EOC,exp}}}{p_{\mathrm{EOC,exp}}} = \left(1 + \frac{\gamma_\mathrm{EOC}-1}{2} M^2_\mathrm{EOC} \right)^{\frac{\gamma_\mathrm{EOC}}{\gamma_\mathrm{EOC}-1}} \tag{5}$$

The total pressure loss due to the acceleration of the combustion gases from zero velocity to M_{EOC} is calculated according to[3]

$$\frac{p_{0,\mathrm{theo}}}{p_{0,\mathrm{EOC,theo}}} = \frac{1 + \gamma_{\mathrm{EOC}} M_{\mathrm{EOC}}^2}{\left(1 + \frac{\gamma_{\mathrm{EOC}}-1}{2}\right)^{\frac{\gamma_{\mathrm{EOC}}}{\gamma_{\mathrm{EOC}}-1}}} \tag{6}$$

Combining equations (3),(5) and (6) results in

$$\eta_{c^*} = \frac{p_{\mathrm{EOC,exp}}}{p_{0,\mathrm{theo}}} \left(1 + \gamma_{\mathrm{EOC}} M_{\mathrm{EOC}}^2\right) \tag{7}$$

The combustion efficiency is calculated using (7), the static pressure at the location EOC and the propellant mass flow rates and temperatures measured during the hot run for the determination of $p_{0,\mathrm{theo}}$. For a detailed analysis several loss factors have to be taken into account.

- Pressure losses due to wall friction are not considered in this analysis.
- A considerable amount of heat is lost due to the cooling of the combustion chamber segments. This amount is in the range of 5 % of total released heat. The quantification of the effect of the heat loss on the total pressure profile in the combustion chamber requires a detailed analysis. The equilibrium composition of the combustion gases changes in axial direction, while the heat capacity of the mixture varies accordingly. At the same time the heat transfer to the wall is a function of the axial distance. Such a detailed analysis is beyond the skope of this work. The assumption of adiabatic walls leads to a maximum total temperature and pressure for the estimation of the ideal total chamber pressure and therefore to the most conservative estimate for the combustion efficiency. In order to keep the heat flux variations during a test at a minimum, the cooling water mass flow rate was nearly proportional to the propellant mass flow rate and thus the chamber pressure. This allows for a comparison of different operating conditions during one test run in respect to the heat losses due to cooling.
- At the test facility P8 oxygen is pressurized using nitrogen, which results in a change in the equilibrium composition. The measured mass flow rate for oxygen includes a certain percentage of nitrogen, which does not contribute to the energy release during combustion. Assuming an oxygen mass fraction of unity leads to the maximum theoretical total chamber pressure and to the minimum combustion efficiency since $\eta_{c^*} = p_{0,\mathrm{exp}}/p_{0,\mathrm{theo}}$. A simple correction factor for the combustion efficiency is calculated as a function of oxygen mass fraction and theoretical total chamber pressure using CEA. Results are shown in figure 3 for a hydrogen temperature of 50 K. For the test runs presented here, measurements indicate an oxygen mass fraction between 95 % and 97 %. This correction factor is not included in the presented values for the combustion efficiency.

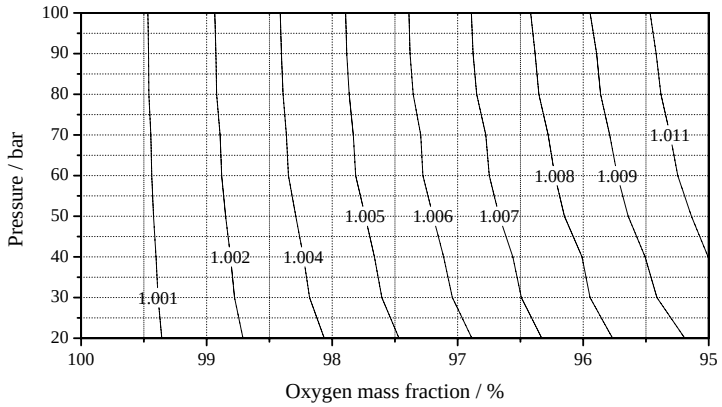

Figure 3: Correction factor for the nitrogen mass fraction

- The exact value of the nozzle throat diameter during hot run is an uncertainty in the calculation of the theoretical total chamber pressure which determines the combustion efficiency. During the hot run the heat load to the nozzle wall causes a thermal strain and the nozzle geometry is changing. This thermal strain, the pressure loads and the restraint due to the outer supporting structure of the combustion chamber determine the change in nozzle throat diameter. A quantitative analysis of the resulting change in nozzle throat diameter requires the use of FEM. This task was not performed for the calculation of the data presented here. The nozzle throat diameter used for the calculation of the combustion efficiency was 28 mm. A detailed analysis of the influence of the heat load on the nozzle geometry is planned for the near future.

3.1.2 Results

The combustion efficiency was calculated for the pressure ramps described in section 2.2. The results are presented in figure 4. The bigger symbols represent the values of the stationary operating conditions just before and after the pressure ramp. For pressure ramp I ($T_{H_2} \approx 50\,\mathrm{K}$) η_{c^*} ranges from 94 % to 97 % with increasing theoretical total chamber pressure. The pressure ramps II and III with $T_{H_2} \approx 105\,\mathrm{K}$ show the opposite trend, but less pronounced. Values range from 99 % to 97.5 %. Comparing the combustion efficiencies of the stationary operating conditions shows that for pressure ramps II and III combustion efficiencies are essentially the same for 30 bar and 100 bar, respectively. For the pressure ramp I the difference in combustion efficiency between the lower and upper operating point is also lower than the span of the values for the pressure ramp itself. This effect can be attributed to the dynamic behaviour of the P8 test bench. The mass flow measurement, which is used to calculate the theoretical total chamber pressure, is located at least 6.5 m away from the injector head. For a pressure ramp with positive pressure increment like the pressure ramp I the actual mass flow rate at a certain time at the injector head is less than the measured one. This leads to a negative bias for the calculation of the combustion efficiency. In case of pressure ramps II and III with decreasing chamber pressure the same effect leads to a positive bias. The comparison between pressure ramp I and the corresponding steady state operating points shows that this bias is stronger at low chamber pressures. For constant-rate pressure ramps the pressure ratio between two points in time and therefore the deviation of actual mass flow rate to measured mass flow rate is larger at lower absolute pressures. Pressure ramps II and III were performed with a pressure change rate of -1 bar/s, while pressure ramp I had a rate of 2 bar/s, leading to a more pronounced dynamic bias for pressure ramp I.
For a quantitative determination of this bias, a detailed analysis of the filling processes encountered during the transient phases has to be performed. A transfer function including the various different hydraulic elements between the position of the mass flow measurement and the injector head faceplate is needed. This is beyond the scope of this publication. Yet, it can be assumed that the correction of this dynamic bias would lead to lower η_{c^*} efficiencies for pressure ramps II and III and higher η_{c^*} efficiencies for pressure ramp I. Since the effect of the dynamic bias is stronger at lower chamber pressures, a correction of the dynamic bias results in a weaker pressure dependency of the η_{c^*} efficiency.

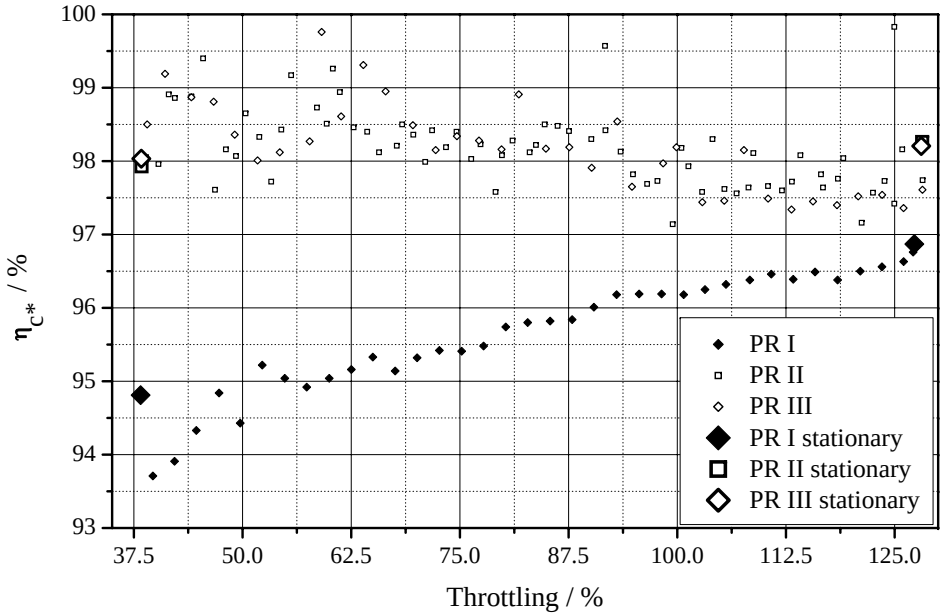

Figure 4: Calculated η_{c^*} efficiencies

3.2 Combustion Stability

The use of dynamic pressure sensors for the test runs performed allows for the determination of combustion stability over the range of operating conditions described above. Combustion stability is most commonly determined using dynamic pressure readings. Pressure oscillations below 5 % of static chamber pressure indicate a smooth combustion, while pressure oscillations exceeding this value are considered a rough combustion.[5] Figure 5 shows the absolute values for the dynamic pressure normalized by a sliding average of a static pressure measured directly behind the

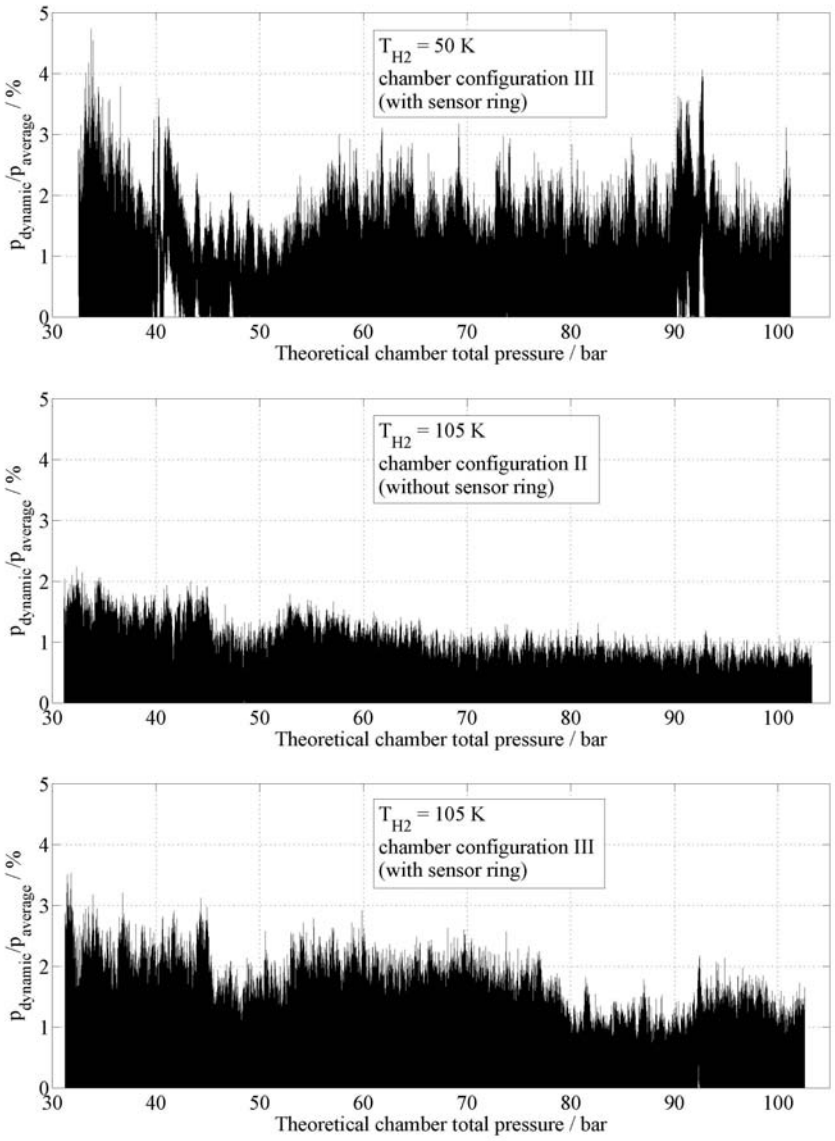

Figure 5: Combustion roughness for pressure ramp I-III (top to bottom)

injector face. For all pressure ramps investigated the combustion roughness is below 5 % for the whole range of the individual pressure ramp. The difference in amplitude between PR II and PR III can be attributed to the dampening effect of the gas volume enclosed in the tubes used for the dynamic pressure sensors in configuration II (see 2.1). During PR II and PR III combustion roughness increases towards lower chamber pressures. Such a clear trend can not be observed for PR I, although the highest combustion roughness occurs at low chamber pressures around 30 bar. All pressure ramps show a slight decrease in combustion roughness around 50 bar theoretical total chamber pressure, which is in the proximity of the critical pressure for oxygen.
A preliminary spectrum analysis showed no distinct exitation of characteristic chamber frequencies or their over tones (see table 2). Instead, dominant frequencies have been observed in the range of 40-100 Hz. The test facility P8 is known to introduce frequencies in this range via the propellant feed lines.

3.3 Wall Heat Flux

Wall heat fluxes are determined using the cooling water mass flow rate for each individual segment and the corresponding temperature change. For a segment in thermal equilibrium this measured value is equal to the heat flux at the combustion chamber wall. For the steady state points of PR I and PR III wall heat fluxes normalized by their individual maximum value are given in figure 6. The data points at $x = 339$ mm represent the nozzle throat position. For identical pressure levels the normalized heat fluxes for PR I in the cylindrical chamber section are lower than those for PR III.

This can be explained by the lower combustion efficiency measured for the 50 K ramp. For PR I more unburned oxidizer is present in the nozzle section than for PR III. This oxidizer is able to react in the nozzle section, which increases the heat loads to the nozzle wall, therefore increasing the ratio between nozzle section and cylindrical part.

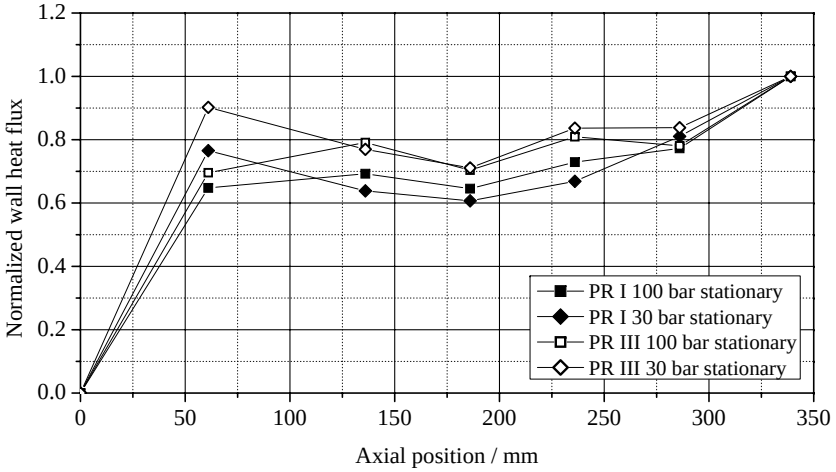

Figure 6: Wall heat fluxes determined for the steady state points of PR I and PR III

4. Conclusion

The operation of a porous injector using the API design has been demonstrated using LOX/H_2. The chamber pressure has been varied over a broad throttling range of 37.5 % to 125 % of nominal chamber pressure (80 bar). The test runs were performed using a 50 mm diameter modular combustion chamber. The lowest hydrogen injection temperature was 50 K. The combustion efficiency has been calculated for the transient and stationary phases. Uncorrected values for the combustion efficiency at a hydrogen injection temperature of 105 K ranged from 99.5 % to 98.5 % and from 94 % to 97 % for a hydrogen injection temperature of 50 K. The pressure dependency of these values is expected to decrease after application of a suitable correction for the dynamic behaviour of the P8 test bench. Combustion roughness was measured directly behind the faceplate and was below 5 % of the mean chamber pressure at all conditions. The combustion is therefore considered a smooth combustion. The wall heat fluxes have been determined using a calorimetric method. Heat fluxes close to the injector head are comparable to those further downstream. This indicates an onset of the combustion region close to the injector head.
The data presented indicate that a porous injector head of API design is well suited for applications requiring deep throttling which results in a drastic change of the injection conditions. In terms of the combustion efficiency and stability, the new injector head design presented here shows a low sensitivity regarding changing injection conditions.

Acknowledgements

The authors would like to thank the P8 team for their contributions to the success of the presented test campaign.

References

[1] Dressler, G. A. and Bauer, J. M.: TRW pintle engine heritage and performance characteristics. In: *36th AIAA/ASME/SAE/ASEE Joint Propulsion Conference and Exhibit*, Huntsville, 2000

[2] Lux, J., Suslov, D. and Haidn, O. J.: Near-critical injection in cryogenic liquid propellant rocket engines using a porous injector head arrangement. In: *ILASS Americas*, Orlando, 2008

[3] Sutton, G. P. and Biblarz, O.: Rocket Propulsion Elements, 3th Edition. John Wiley & Sons, 1963

[4] Sutton, G. P. and Biblarz, O.: Rocket Propulsion Elements, 7th Edition. John Wiley & Sons, 2001

[5] Harrje, T. P.: Liquid Propellant Rocket Combustion Instability, NASA SP-194, Washington D.C., 1972